

Probing Nonlocal Spatial Correlations in Quantum Gases with Ultra-long-range Rydberg Molecules

J. D. Whalen,¹ S. K. Kanungo,¹ R. Ding,¹ M. Wagner,^{2,3} R. Schmidt,^{2,3} H. R. Sadeghpour,⁴ S. Yoshida,⁵ J. Burgdörfer,⁵ F. B. Dunning,¹ and T. C. Killian^{1,*}

¹*Department of Physics & Astronomy and Rice Center for Quantum Materials, Rice University, Houston, TX 77251, USA*

²*Max-Planck-Institute of Quantum Optics, Hans-Kopfermann-Strasse 1, 85748 Garching, Germany*

³*Munich Center for Quantum Science and Technology, Schellingstraße 4, D-80799 München, Germany*

⁴*ITAMP, Harvard-Smithsonian Center for Astrophysics, Cambridge, MA 02138, USA*

⁵*Institute for Theoretical Physics, Vienna University of Technology, Vienna, Austria, EU*

(Dated: March 28, 2019)

We present photo-excitation of ultra-long-range Rydberg molecules as a probe of spatial correlations in quantum gases. Rydberg molecules can be created with well-defined internuclear spacing, set by the radius of the outer lobe of the Rydberg electron wavefunction R_n . By varying the principal quantum number n of the target Rydberg state, the molecular excitation rate can be used to map the pair-correlation function of the trapped gas $g^{(2)}(R_n)$. We demonstrate this with ultracold Sr gases and probe pair-separation length scales ranging from $R_n = 1400 - 3200 a_0$, which are on the order of the thermal de Broglie wavelength for temperatures around $1 \mu\text{K}$. We observe bunching for a single-component Bose gas of ^{84}Sr and anti-bunching due to Pauli exclusion at short distances for a polarized Fermi gas of ^{87}Sr , revealing the effects of quantum statistics.

Our understanding of quantum gases has been greatly enhanced by *in situ* measurements of spatial correlations, which can arise from Bose or Fermi quantum statistics [1–5] or the formation of more complex entangled states [6–8]. Quantum gas microscopes resolve correlations on length scales on the order of, or larger than a wavelength of light, enabling studies of quantum magnetism [9] and the superfluid-to-Mott insulator transition [10]. Inelastic loss from spin flips and three-body recombination probe two- and three-body spatial correlations at very short range [2, 7]. Despite the tremendous progress in experimental techniques, *in situ* probes of spatial correlations between these length scales are still lacking. Many complex many-body phenomena take place at these intermediate scales, and such a probe would thus provide a new window into physics such as the formation of halo dimers [11] and Efimov trimers [12] related to resonant atomic scattering states, long-range Cooper pairs in strongly interacting Fermi gases [13, 14], and strongly correlated 1D gases [7, 8].

Here we demonstrate photo-excitation of ultra-long-range Rydberg-molecule (RM) dimers [15–17] in an ultracold gas as an *in situ* probe of nonlocal pair-correlations [1] at previously inaccessible length scales. At short range, we observe bunching in a thermal gas of spinless bosonic ^{84}Sr and Pauli exclusion, or anti-bunching, in a polarized gas of fermionic ^{87}Sr atoms, reflecting the effects of (anti-)symmetrization of the wave functions dictated by the spin statistics theorem. These correlations vanish at distances greater than the thermal de Broglie wavelength. Bunching and anti-bunching have been observed before in quantum gases with destructive mea-

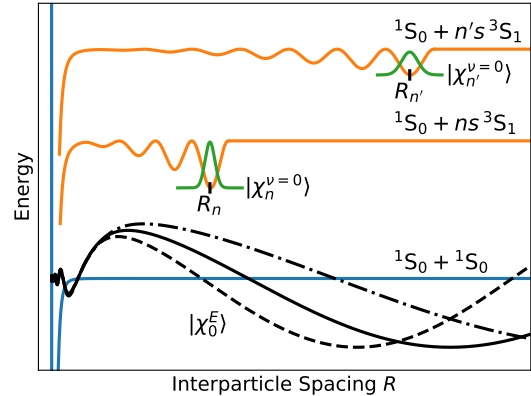


FIG. 1. Schematic of the excitation to a Rydberg molecular state $|\chi_n^{\nu=0}\rangle$ (green) in a Rydberg potential (orange) from the state of a pair of colliding atoms $|\chi_0^E\rangle$ (black). The wavefunction of the ground $\nu = 0$ molecular dimer state is highly localized in the outer lobe of the molecular potential at R_n , as shown for two different principal quantum numbers n and n' . Asymptotically far outside the short-range interatomic potential (blue), $|\chi_0^E\rangle$ describes a free particle state with wave vector $k = \sqrt{2\mu E/\hbar^2}$ for collision energy E and reduced mass μ . The experiment samples a thermal distribution of collision energies, and the molecular excitation rate is proportional to the pair correlation function $g^{(2)}(R_n)$.

surement schemes [2, 5, 18–21]. In contrast, RM excitation can be nearly non-destructive [22]. It can also probe the temporal evolution of correlations since the molecular binding energy, and therefore the inverse excitation time scale, are much greater than the relevant many-body energy scales of quantum gases, such as the Fermi energy or chemical potential.

In a RM dimer, one ground-state atom is bound to a

* corresponding author: killian@rice.edu

highly excited Rydberg atom. The binding potential results from scattering between the Rydberg electron and ground-state atom [15, 23], and it therefore follows the Rydberg-electron probability distribution. (See Fig. 1.) For Sr, the atom-electron interaction is attractive, leading to formation of RMs. The molecular potential is also attractive for Rydberg excitations in Rb and Cs quantum gases [16, 24, 25], which attests to the broad applicability of the probe we investigate in the present work.

To probe spatial correlations, we exploit the fact that the internuclear separation in the most deeply bound RM dimer state, $|\chi_n^{\nu=0}\rangle$, is highly localized in the potential minimum formed by the outer lobe of the Rydberg wavefunction located at a separation $R_n \approx 2(n - \delta)^2 a_0$ (Fig. 1). The quantum defect is $\delta = 3.37$ for the $5sns^3S_1$ states used in this work, and $a_0 \approx 0.05$ nm is the Bohr radius. In a simple semi-classical picture, the formation of a molecule requires the presence of atoms separated by approximately R_n . Thus the excitation rate serves as a measure of the relative probability of finding two particles with separation R_n in the initial gas, which can be quantified by the nonlocal pair-correlation function $g^{(2)}(R_n)$. For principal quantum number n between 20 and 75, R_n ranges from 400 to $10^4 a_0$, providing an *in situ* probe of correlations at previously inaccessible length scales. This method is similar to the mapping of short-range ($\lesssim 100 a_0$) atomic scattering states with photoassociative spectroscopy of low-lying energy levels [26–30]. The possibility of measuring non-local correlations with RMs was mentioned in [31], and short-range correlations were probed with RM excitation in [22].

In the present work, non-degenerate quantum gases of spin-polarized, fermionic ^{87}Sr ($I = 9/2$) and bosonic ^{84}Sr ($I = 0$) are used to measure the effects of quantum statistics on the excitation rate of RMs and thus on the pair correlation function. As a reference, we employ an unpolarized sample of ^{87}Sr , which provides a good approximation to a gas of uncorrelated particles because of its tenfold-degenerate ground state. Accordingly, the excitation rates of RMs in ^{84}Sr and spin-polarized ^{87}Sr are compared to those of unpolarized ^{87}Sr to extract $g^{(2)}(R)$.

Ultracold samples of bosonic ^{84}Sr are produced by loading a magneto-optical trap (MOT) operating on the $5s^2^1S_0 \rightarrow 5s5p^1P_1$ transition at 461 nm. Weak spontaneous decay from the $5s5p^1P_1$ state transfers atoms into the metastable $5s5p^3P_2$ state, a fraction of which are magnetically trapped by the quadrupole magnetic field of the MOT [32]. Magnetically trapped atoms are then returned to the ground state using optical pumping on the $5s5p^3P_2 \rightarrow 5p^2^3P_2$ transition at 481 nm [33]. Atoms are further cooled to $\sim 2 \mu\text{K}$ using a second MOT operating on the $5s^2^1S_0 \rightarrow 5s5p^3P_1$ intercombination line ($\Gamma/2\pi = 7.5$ kHz) at 689 nm. Subsequently, the atoms are loaded into an optical dipole trap (ODT) formed using 1064 nm light and evaporatively cooled to the desired temperature.

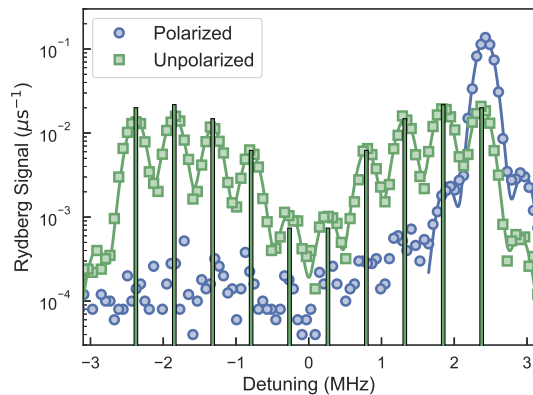


FIG. 2. Spectra for excitation to the atomic $n = 34$ Rydberg state for spin-polarized (circles) and unpolarized (squares) gases of ^{87}Sr . A 1 G magnetic field causes the observed Zeeman splitting. The vertical bars indicate the square of Clebsch-Gordan coefficients associated with each transition, and differences with the measured peak heights point to small deviations from an equal distribution of m_F levels in the ground state. Curves show fits used to extract the population in each m_F level. The small features on the extreme right and extreme left of the plot arise due to imperfect polarization of the first photon, and are included in the model for completeness.

To produce samples of fermionic ^{87}Sr , metastable $5s5p^3P_2$ ^{84}Sr and ^{87}Sr atoms are sequentially loaded into the magnetic trap. Both isotopes are repumped simultaneously using 481 nm light, after which they are further cooled to $\sim 2 \mu\text{K}$ in a simultaneous dual-isotope narrow-line MOT and loaded into the ODT.

For measurements involving spin-polarized ^{87}Sr , a bias magnetic field of 7.6 G is applied after loading the ODT, which produces a Zeeman splitting of ~ 650 kHz between adjacent magnetic sublevels in the $5s5p^3P_1$ $F = 9/2$ manifold. Population is transferred into the $m_F = 9/2$ ground state by applying a series of σ^+ polarized 689 nm laser pulses approximately 50 kHz red-detuned from each $m_F \rightarrow m_F + 1$ transition. Once this optical pumping is complete, the field is lowered to ~ 1 G to maintain the quantization axis. Experiments with unpolarized samples are performed in zero magnetic field.

After a ^{87}Sr sample is prepared in the appropriate state, it is evaporatively cooled by lowering the optical trap depth over a period of several seconds. The presence of ^{84}Sr allows for sympathetic cooling of polarized ^{87}Sr atoms, and yields colder samples of unpolarized ^{87}Sr atoms. Once the final trap depth is reached, any remaining ^{84}Sr atoms are removed by scattering light resonant with the $5s^2^1S_0 \rightarrow 5s5p^3P_1$ transition. The isotope shift between ^{87}Sr and ^{84}Sr ensures that no significant heating of the ^{87}Sr atoms occurs.

A two-photon transition is employed to create Rydberg atoms or molecules. The first photon, at 689 nm, has a fixed blue-detuning of 14 MHz from the $5s5p^3P_1$

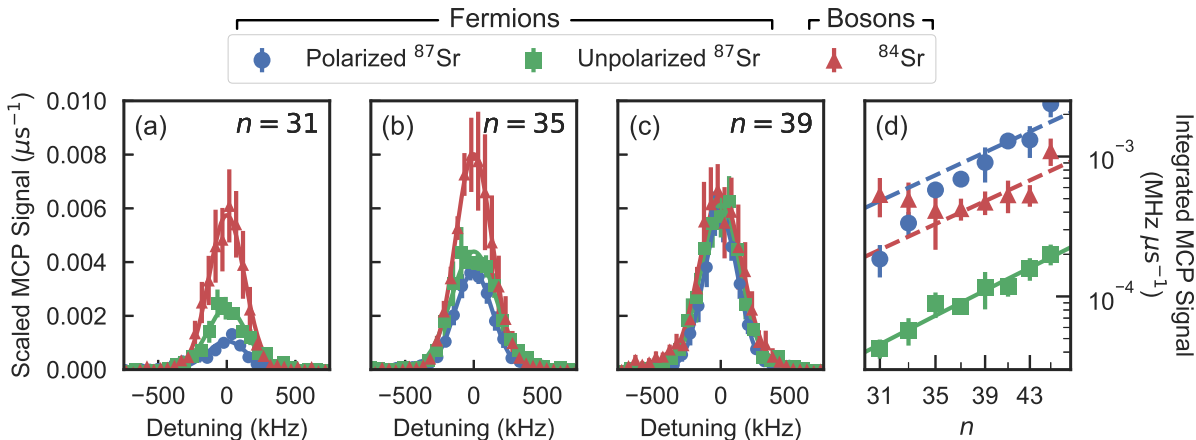


FIG. 3. Raw data showing the effects of quantum statistics on the excitation of RMs. (a-c) Spectra for excitation to the $|\chi_n^{\nu=0}\rangle$ dimer ground state for a spin-polarized ^{87}Sr Fermi gas (blue, circles), for an unpolarized ^{87}Sr Fermi gas (green, squares) and a spinless ^{84}Sr Bose gas (red, triangles). The spectra for the polarized Fermi gas and the spinless Bose gas are scaled such that the spectra match at $n = 39$ to highlight the effects of quantum statistics (see text). (d) Integrated signal of the RM spectra versus principal quantum number. A fit (solid green line) shows that the integral for the unpolarized gas varies as $(n - \delta)^\alpha$, with $\alpha = 3.5(3)$, reflecting variation in the n -dependent Franck-Condon factors and electronic matrix element, with some contribution from faster natural decay at lower n . The dashed lines are translations of the $(n - \delta)^\alpha$ curve to guide the eye.

level ($F = 11/2$ for ^{87}Sr). The energy of the second photon, at 320 nm, is scanned to obtain spectra for excitation to $5sns\ ^3S_1$ levels ($F = 11/2$ for ^{87}Sr) (Figs. 2 and 3). The excitation lasers are applied for 10 μs , after which an electric field is applied to ionize Rydberg excitations. Product electrons are counted using a microchannel plate detector. Typically, 1000 laser pulses at a single frequency are applied to each sample.

To quantitatively measure the pair-correlation function $g^{(2)}(R)$, the molecular excitation rate in a correlated gas is normalized with respect to the rate in an uncorrelated gas. This allows us to cancel experimental factors and, most importantly, n -dependent contributions to the excitation rate that are unrelated to spatial correlations. Maintaining similar sample densities and temperatures increases the accuracy of this procedure. To this end, we approximately match the final trap potential, excitation laser intensity, atom number, peak density, and sample temperature. The latter quantities are inferred from time-of-flight absorption imaging on the $5s^2\ ^1S_0 \rightarrow 5s5p\ ^1P_1$ transition at 461 nm and knowledge of the trapping potential [34].

The effectiveness of optical pumping is measured spectroscopically through excitation of the $5sns\ ^3S_1$ $F = 11/2$ atomic Rydberg state in a 1 G magnetic field using two π -polarized photons ($\Delta m_F = 0$). The spectrum (Fig. 2) is fit to an appropriate lineshape model to determine the degree of polarization. For a polarized sample, at least 90% of the atoms occupy the $m_F = 9/2$ state. For the unpolarized Fermi gas, the populations in the ten different ground-state m_F levels are approximately equal

($\pm 25\%$). The differing heights of the Zeeman peaks in the spectrum for the unpolarized sample arise from the variation of transition strength from the ground state to final states with different magnetic quantum numbers as given by angular momentum coupling (Clebsch-Gordan coefficients).

To probe spatial correlations and measure $g^{(2)}(R)$, a polarization configuration different from the one used to probe polarization is used to create Rydberg molecules. The first photon is σ^+ polarized, and the second photon remains π polarized, which maximizes the transition strength for the spin-polarized sample.

The influence of quantum statistics on spatial correlations is readily apparent in the spectra for excitation to the $\nu = 0$ RM state at principal quantum numbers $31 \leq n \leq 45$ ($1400 a_0 \leq R_n \leq 3200 a_0$). Figures 3(a-c) show spectra for $n = 31, 35, 39$. The spectra for the spin-polarized Fermi gas ($T = 650\text{ nK}$) and Bose gas ($T = 860\text{ nK}$) are scaled such that their integrals match the integral of the unpolarized data ($T = 860\text{ nK}$) at $n = 39$, where the effects of quantum statistics are small [Fig. 3(c)]. For decreasing quantum number [Fig. 3(a,b)], the suppression of the excitation rate in the spin-polarized Fermi gas arising from Pauli exclusion and the enhancement for the Bose gas due to bunching are evident.

Figure 3(d) shows the integral of the molecular signals measured for each principal quantum number. The integrals for the unpolarized Fermi gas (green circles) can be fit well by an $(n - \delta)^{3.5}$ power law. In the absence of effects of quantum statistics, the integrals for all samples

should have the same n dependence but different overall amplitudes that reflect n -independent factors such as Clebsch-Gordan coefficients (Fig. 2), differences in detector efficiency arising from the magnetic field needed to preserve quantization for the spin-polarized sample, and differences in laser intensity between the Bose and spin-polarized Fermi gas experiments. Deviations from the $(n - \delta)^{3.5}$ power law at low quantum number result from quantum statistics.

The excitation probability to the ground vibrational state ($\nu = 0$) of the RM for principal quantum number n is proportional to a Franck-Condon factor that accounts for a thermal average over collision energy $\langle (\dots)_E \rangle$ for initial two-particle states and all possible initial and final rotational states. This reduces to $\mathcal{F}_n = \sum_l (2l + 1) \langle |\int dR R^2 \chi_n^{\nu=0}(R) \chi_0^{E,l}(R)|^2 \rangle_E$ [35], where $\chi_n^{\nu=0}$ is the radial wavefunction for the RM, which is independent of l for the low- l states contributing to \mathcal{F}_n . $\chi_0^{E,l}$ is the wavefunction for the initial state with collisional energy E and rotational angular momentum quantum number l . The sum over l is understood to be restricted to initial states with allowed exchange symmetry.

$\chi_n^{\nu=0}$ is well-localized at R_n on the scale of the initial collisional state. In particular, the wave function for $n < 50$ is localized within a single potential well (Fig. 1). This allows \mathcal{F}_n to be approximated as [35]

$$\mathcal{F}_n \simeq \left| \int dR R^2 \chi_n^{\nu=0}(R) \right|^2 g^{(2)}(R_n) \equiv \mathcal{O}_n g^{(2)}(R_n) \quad (1)$$

where $g^{(2)}(R_n)$ is the pair correlation function for separation R_n , and \mathcal{O}_n is an effective Franck-Condon factor. This derivation can be generalized to the case of an initial state of a many-body Fermi or Bose gas at arbitrary density and temperature and with multiple internal spin states initially populated.

When experimental factors are taken into account, the integrated signal becomes

$$\mathcal{S}_n \simeq \alpha I_1 I_2 \mathcal{N} \beta_n \mathcal{O}_n C g^{(2)}(R_n), \quad (2)$$

which is proportional to the detector efficiency α , the two-photon-excitation laser intensities I_1 and I_2 , the volume integral of the square of the density distribution $\mathcal{N} \equiv \int d^3r \rho(\mathbf{r})^2$, a factor β_n proportional to the square of the reduced two-photon electronic-transition matrix element, a factor C expressible in terms of Clebsch-Gordan coefficients, \mathcal{O}_n , and $g^{(2)}(R_n)$.

For non-degenerate gases of noninteracting particles, $g^{(2)}(R)$ should be given by

$$g^{(2)}(R) = 1 + \epsilon e^{-2\pi R^2/\lambda_{\text{dB}}^2}, \quad (3)$$

where $\lambda_{\text{dB}} = h/\sqrt{2\pi m k_B T}$ is the thermal de Broglie wavelength, and ϵ equals $+/-1$ for indistinguishable thermal bosons/fermions in identical internal states and

0 for classical statistics [1, 36]. Trap and phase-space-density-dependent corrections to Eq. (3) will vary with separation R and are always less than $z/10$ [1], where $z \approx \rho \lambda_{\text{dB}}^3$ is the fugacity. The highest peak fugacity of any of the samples used in these experiments is $z = 0.4$, and corrections are small. Eq. (3) neglects interactions between ground-state particles, which modify spatial correlations at length scales less than the scattering length or the range of the ground-state atom-atom molecular potential, which are much smaller than R_n probed in this experiment.

Equation (2) is used to experimentally determine $g^{(2)}(R_n)$ for indistinguishable particles in identical internal states by normalizing the integrated signals for the bosons and spin-polarized fermions to the integrated signal for the unpolarized fermions. This cancels common factors β_n and \mathcal{O}_n . For the unpolarized Fermi gas, we assume $g^{(2)}(R) = 1 - 0.1e^{-2\pi R^2/\lambda_{\text{dB}}^2}$, which is the generalization of Eq. (3) for equal populations in the ten ground spin-states. The remaining factors that vary between different experimental runs and different isotopes and sample polarizations, are either measured or calculated independently. The Clebsch-Gordan factor for the unpolarized gas (C_{unpol}) is calculated assuming equal populations in all ground spin states, yielding $C_{\text{pol}}/C_{\text{unpol}} = 5.05$, where C_{pol} describes bosons and polarized fermions. Temperatures and densities (peak density $\sim 3 \times 10^{13} \text{ cm}^{-3}$) of each sample and the unpolarized gas used for normalization match within 10% in all cases. For the Bose gas, $T/T_c \approx 1.5$ where T_c is the critical temperature for Bose condensation. For the polarized Fermi gases, $T/T_F \approx 1.0$, where T_F is the Fermi temperature. For the unpolarized Fermi gases, $T/T_F \approx 2$. Density distributions are calculated using the appropriate Bose or Fermi distributions.

At large separations, where the effect of quantum statistics should be negligible, this procedure yields $g^{(2)}(R) = 1.5$ rather than the expected value of 1. A systematic deviation of this size is consistent with uncertainties in relative populations of the initial internal spin states of the unpolarized Fermi gas and in trap geometry and resulting density profiles. Ratios are thus divided by an additional correction factor of 1.5 to obtain the values of $g^{(2)}(R_n)$ in Fig. 4.

At lower values of n the normalized integrated signals for the bosons and fermions clearly deviate from unity (Fig. 4(a)). The boson signal increases while the fermion signal decreases, which is consistent with bunching and anti-bunching respectively. The Fermi-gas experiment was performed at two different temperatures, and anti-bunching is less pronounced in the warmer sample reflecting the shorter thermal de Broglie wavelength. Figure 4 also shows that the results follow the expected behavior for $g^{(2)}(R)$ (Eq. (3)).

On a scaled, dimensionless axis (Fig. 4(b)), the two fermionic data sets fall on the same curve and approach

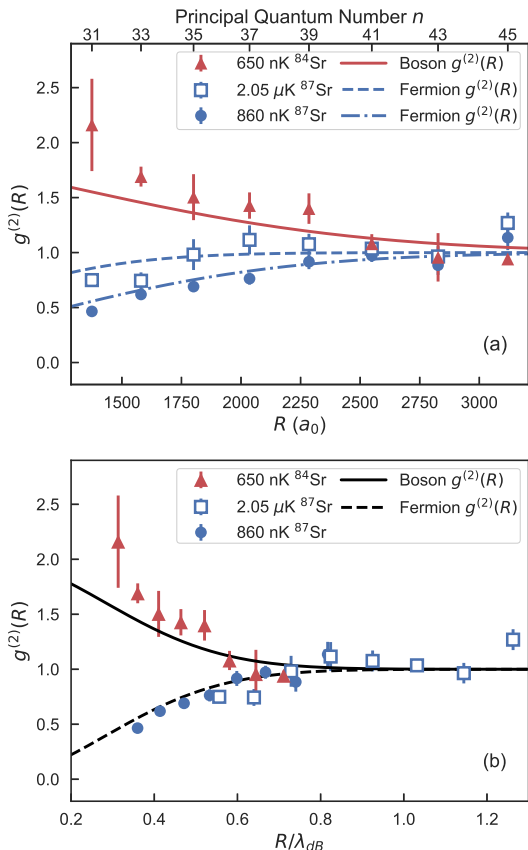


FIG. 4. Measured pair-correlation function for indistinguishable particles in identical internal states. (a) $g^{(2)}(R)$ for a Bose gas and Fermi gases at two different temperatures plotted against interparticle separation, R_n . Sample temperatures are indicated in the legend. (b) $g^{(2)}(R)$ for Fermi and Bose gases plotted against R_n scaled by the thermal de Broglie wavelength. The two sets of fermion measurements (blue symbols) fall onto a single curve and approach a constant value at large scaled distances. Error bars indicate statistical fluctuations from repeated measurements. Expected $g^{(2)}(R)$ (Eq. (3)) for bosons (solid) and fermions (dashed and dot-dashed) are shown by the lines.

a constant value for larger R/λ_{dB} . Effects of quantum statistics - bunching for bosons and anti-bunching due to Pauli exclusion for fermions - are strikingly evident.

In summary, we have demonstrated that photoexcitation of the most deeply bound, $\nu = 0$ dimer RM state provides an *in situ* probe of pair-correlations in an ultracold gas that can be tuned over previously inaccessible length scales. These results suggest other interesting phenomena that can be studied with this diagnostic. For example, the pair-correlation function in a gas with a large s-wave scattering length, in the range of R_n probed in this experiment, should show strong deviations from the non-interacting result presented in Eq. (3). Stronger suppression/enhancement effects on higher-order correlations should be observable with trimers, tetramers,

etc. Moreover, due to the fact that Rydberg molecule formation takes place on a time scale ($\sim 1 \mu\text{s}$) much faster than the relevant many-body dynamics of quantum gases, RMs hold promise for *in situ* probing of the time evolution of correlations during the non-equilibrium dynamics following quantum quenches or in driven many-body systems.

Acknowledgements: Research supported by the AFOSR (FA9550-14-1-0007), the NSF (1301773, 1600059, and 1205946), the Robert A. Welch Foundation (C-0734 and C-1844), the FWF (Austria) (FWF-SFB041 ViCoM, and FWF-SFB049 NextLite). The Vienna scientific cluster was used for the calculations. H. R. S. was supported by the NSF through a grant for the Institute for Theoretical Atomic, Molecular, and Optical Physics at Harvard University and the Smithsonian Astrophysical Observatory. R. S. and M. W. were supported by the Deutsche Forschungsgemeinschaft (DFG, German Research Foundation) under Germanys Excellence Strategy EXC-2111 390814868.

-
- [1] M. Naraschewski and R. J. Glauber, Phys. Rev. A **59**, 4595 (1999).
 - [2] E. A. Burt, R. W. Ghrist, C. J. Myatt, M. J. Holland, E. A. Cornell, and C. E. Wieman, Phys. Rev. Lett. **79**, 337 (1997).
 - [3] W. Ketterle and H.-J. Miesner, Phys. Rev. A **56**, 3291 (1997).
 - [4] M. W. Zwierlein, Z. Hadzibabic, S. Gupta, and W. Ketterle, Phys. Rev. Lett. **91**, 250404 (2003).
 - [5] A. Omran, M. Boll, T. A. Hilker, K. Kleinlein, G. Salomon, I. Bloch, and C. Gross, Phys. Rev. Lett. **115**, 1 (2015).
 - [6] I. Bloch, J. Dalibard, and W. Zwerger, Rev. Mod. Phys. **80**, 885 (2008).
 - [7] B. Laburthe Tolra, K. O'Hara, J. Huckans, W. Phillips, S. Rolston, and J. Porto, Phys. Rev. Lett. **92**, 190401 (2004).
 - [8] T. Kinoshita, T. Wenger, and D. S. Weiss, Science **305**, 1125 (2004).
 - [9] A. Mazurenko, C. S. Chiu, G. Ji, M. F. Parsons, M. Kanász-Nagy, R. Schmidt, F. Grusdt, E. Demler, D. Greif, and M. Greiner, Nature (London) **545**, 462 EP (2017).
 - [10] W. S. Bakr, A. Peng, M. E. Tai, R. Ma, J. Simon, J. I. Gillen, S. Fölling, L. Pollet, and M. Greiner, Science **329**, 547 (2010).
 - [11] T. Köhler, K. Góral, and P. S. Julienne, Rev. Mod. Phys. **78**, 1311 (2006).
 - [12] C. Chin, R. Grimm, P. Julienne, and E. Tiesinga, Rev. Mod. Phys. **82**, 1225 (2010).
 - [13] E. Altman, E. Demler, and M. Lukin, Phys. Rev. A **70**, 013603 (2004).
 - [14] S. Giorgini, L. P. Pitaevskii, and S. Stringari, Rev. Mod. Phys. **80**, 1215 (2008).
 - [15] C. Greene, A. Dickinson, and H. Sadeghpour, Phys. Rev. Lett. **85**, 2458 (2000).
 - [16] V. Bendkowsky, B. Butscher, J. Nipper,

- J. P. Shaffer, R. Löw, and T. Pfau, *Nature (London)* **458**, 1005 (2009).
- [17] B. J. Desalvo, J. A. Aman, F. B. Dunning, T. C. Killian, H. R. Sadeghpour, S. Yoshida, and J. Burgdorfer, *Phys. Rev. A* **92**, 031403 (2015).
- [18] M. Schellekens, R. Hoppeler, A. Perrin, J. Viana Gomes, D. Boiron, A. Aspect, and C. I. Westbrook, *Science* **310**, 648 (2005).
- [19] T. Jelte, J. M. McNamara, W. Hogervorst, W. Vassen, V. Krachmalnicoff, M. Schellekens, A. Perrin, H. Chang, D. Boiron, A. Aspect, and C. I. Westbrook, *Nature (London)* **445**, 402 (2007).
- [20] M. Yasuda and F. Shimizu, *Phys. Rev. Lett.* **77**, 3090 (1996).
- [21] T. Rom, T. Best, D. van Oosten, U. Schneider, S. Fölling, B. Paredes, and I. Bloch, *Nature (London)* **444**, 733 (2006).
- [22] T. Manthey, T. Niederprum, O. Thomas, and H. Ott, *New J. Phys.* **17**, 103024 (2015).
- [23] E. Fermi, *Nuovo Cimento* **11**, 157 (1934).
- [24] C. Bahrim, U. Thumm, and I. I. Fabrikant, *J. Phys. B: At. Mol. Opt. Phys.* **34**, 195 (2001).
- [25] D. Booth, S. T. Rittenhouse, J. Yang, H. R. Sadeghpour, and J. P. Shaffer, *Science* **348**, 99 (2015).
- [26] R. Napolitano, J. Weiner, C. Williams, and P. Julienne, *Phys. Rev. Lett.* **73**, 1352 (1994).
- [27] E. R. I. Abraham, W. I. McAlexander, J. M. Gerton, and R. G. Hulet, *Phys. Rev. A* **53**, 3713 (1996).
- [28] E. Tiesinga, C. J. Williams, P. S. Julienne, K. M. Jones, P. D. Lett, and W. D. Phillips, *J. Res. Natl. Inst. Stand. Technol.* **101**, 505 (1996).
- [29] C. Boisseau, E. Audouard, J. Vigué, and P. S. Julienne, *Phys. Rev. A* **62**, 052705 (2000).
- [30] K. Jones, E. Tiesinga, P. Lett, and P. Julienne, *Rev. Mod. Phys.* **78**, 483 (2006).
- [31] M. T. Eiles, *Phys. Rev. A* **98**, 042706 (2018).
- [32] S. B. Nagel, C. E. Simien, S. Laha, P. Gupta, V. S. Ashoka, and T. C. Killian, *Phys. Rev. A* **67**, 011401(R) (2003).
- [33] F. Hu, I. Nosske, L. Couturier, C. Tan, C. Qiao, P. Chen, Y. H. Jiang, B. Zhu, and M. Weidemüller, arXiv:1812.01258.
- [34] S. Stellmer, F. Schreck, and T. C. Killian, in *Annual Review of Cold Atoms and Molecules* (Ed. by K. W. Madison, K. Bongs, L. D. Carr, A. M. Rey, and H. Zhai. World Scientific, Singapore, 2014).
- [35] In preparation.
- [36] D. S. Dean, P. Le Doussal, S. N. Majumdar, and G. Schehr, *Phys. Rev. A* **97**, 063614 (2018).